

See discussions, stats, and author profiles for this publication at: <https://www.researchgate.net/publication/51122972>

Probing Oxygen Activation Sites in Two Flavoprotein Oxidases Using Chloride as an Oxygen Surrogate

ARTICLE *in* BIOCHEMISTRY · JUNE 2011

Impact Factor: 3.02 · DOI: 10.1021/bi200388g · Source: PubMed

CITATIONS

21

READS

28

5 AUTHORS, INCLUDING:



Francis Scott Mathews
Washington University in St. Louis
192 PUBLICATIONS 14,934 CITATIONS

[SEE PROFILE](#)



Marilyn Schuman Jorns
Drexel University College of Medicine
101 PUBLICATIONS 3,083 CITATIONS

[SEE PROFILE](#)



NIH Public Access

Author Manuscript

Biochemistry. Author manuscript; available in PMC 2012 September 22.

Published in final edited form as:
Biochemistry. 2011 June 21; 50(24): 5521–5534. doi:10.1021/bi200388g.

Probing Oxygen Activation Sites in Two Flavoprotein Oxidases Using Chloride as an Oxygen Surrogate†,‡

Phaneeswara-Rao Kommoju[§], Zhi-wei Chen[¶], Robert C. Bruckner[§], F. Scott Mathews^{*,||}, and Marilyn Schuman Jorns^{*,§}

Department of Biochemistry and Molecular Biology, Drexel University College of Medicine, Philadelphia, PA 19102. Department of Biochemistry and Molecular Biology, Saint Louis University School of Medicine, St. Louis, MO 63104. Department of Biochemistry and Molecular Biophysics, Washington University School of Medicine, St. Louis, MO 63110

Abstract

A single basic residue above the *si*-face of the flavin ring is the site of oxygen activation in glucose oxidase (GOX) (His516) and monomeric sarcosine oxidase (MSOX) (Lys265). Crystal structures of both flavoenzymes exhibit a small pocket at the oxygen activation site that might provide a pre-organized binding site for superoxide anion, an obligatory intermediate in the 2-electron reduction of oxygen. Chloride binds at these polar oxygen activation sites, as judged by solution and structural studies. Firstly, chloride forms spectrally detectable complexes with GOX and MSOX. The protonated form of His516 is required for tight binding of chloride to oxidized GOX and for rapid reaction of reduced GOX with oxygen. Formation of a binary MSOX•chloride complex requires Lys265 and is not observed with Lys265Met. Binding of chloride to MSOX does not affect the binding of a sarcosine analog (MTA, methylthioacetate) above the *re*-face of the flavin ring. Definitive evidence is provided by crystal structures determined for a binary MSOX•chloride complex and a ternary MSOX•chloride•MTA complex. Chloride binds in the small pocket at a position otherwise occupied by a water molecule, and forms hydrogen bonds to four ligands that are arranged in approximate tetrahedral geometry: Lys265:NZ, Arg49:NH1 and two water molecules, one of which is hydrogen bonded to FAD:N5. The results show that chloride: (i) acts as an oxygen surrogate; (ii) is an effective probe of polar oxygen activation sites; (iii) provides a valuable complementary tool to the xenon gas method that is used to map nonpolar oxygen-binding cavities.

The 2-electron reduction of molecular oxygen by reduced flavin or other singlet organic molecules may be thermodynamically favorable but is spin-forbidden. Consequently, the reactions proceed via an initial, rate-determining 1-electron step that is spin-allowed but energetically unfavorable. The accelerated rate of oxygen reduction observed with flavoprotein oxidases and other oxidases, including cofactor-less enzymes, is called oxygen

†This work was supported in part by Grant GM 31704 (M. S. J.) from the National Institutes of Health.

‡Crystallographic coordinates have been deposited in the RCSB Protein Data under the file name 3QSM for the MSOX•chloride binary complex, 3QSS for the MSOX•chloride•MTA ternary complex, 3QSE for the reduced MSOX•sarcosine complex, 3QVP for the 1.2 Å resolution GOX structure, and 3QVR for the 1.3 Å resolution GOX structure.

*To whom correspondence and requests for reprints should be addressed. M.S.J.: Phone: (215) 762-7495; FAX: (215) 762-4452; marilyn.jorns@drexelmed.edu. F.S.M.: Phone (314) 362-1080; FAX: (314) 362-7183; mathews@biochem.wustl.edu.

§Drexel University College of Medicine

¶Saint Louis University School of Medicine,

||Washington University School of Medicine

SUPPORTING INFORMATION AVAILABLE

Summary of data collection and refinement for GOX crystals (Table S1), effect of pH on the stability of the complex formed with GOX and chloride (Table S2). This material is available free of charge via the Internet at <http://pubs.acs.org>.

activation (1, 2). Initial formation of a radical pair may be followed by the transfer of a second electron from the organic molecule to the superoxide radical to produce hydrogen peroxide, a path thought to occur in reactions catalyzed by most flavoprotein oxidases. However, in a few flavo-oxidases and in cofactor-less oxidases the radical pair combines to form a peroxy intermediate that subsequently decomposes to yield hydrogen peroxide (3, 4) (Scheme 1).

The kinetics observed for the self-exchange reaction between oxygen and superoxide anion indicate that the reorganization energy required to change the configuration of the surrounding medium (λ_{out}) constitutes the major energy barrier in the 1-electron reduction of oxygen (5). The presence of a pre-organized binding site for superoxide anion in oxidases could decrease λ_{out} and provide a mechanism for accelerating the 1-electron reduction of oxygen. Evidence in support of this hypothesis has been obtained in recent studies with monomeric sarcosine oxidase (MSOX1) (6, 7) and glucose oxidase (GOX) (2, 8, 9).

MSOX is a 44 kDa two-domain flavoprotein that catalyzes the oxidative demethylation of sarcosine (N-methylglycine) and is used in the clinical evaluation of renal function and muscle damage (10–15). MSOX is a prototypical member of a family of amino acid oxidases that contain covalently bound FAD (16–19). Steady-state kinetic studies indicate that oxygen reacts with a reduced MSOX•sarcosine imine complex (12). The active sites for sarcosine oxidation and oxygen reduction in MSOX are on opposite sides of the flavin ring. The sarcosine-binding cavity is located above the *re*-face of the flavin ring (11, 13). Recent mutagenesis studies provide compelling evidence that Lys265 is the site of oxygen activation and that the basic residue is entirely responsible for the enormous rate acceleration observed with wild-type enzyme (6, 7). Lys265 is located above the *si*-face of the flavin ring and forms hydrogen bonds with a pair of active site waters (WAT1, WAT2), one of which is also hydrogen bonded to the N(5) position of FAD (Figure 1A).

GOX is a homodimeric glycoprotein with a molecular weight that varies from 130 to 320 kDa, depending on the extent of glycosylation (20). Each monomer contains two domains and 1 mol of noncovalently bound FAD (21–23). GOX is a member of the glucose-methanol-choline (GMC) family of oxidoreductases that oxidize alcohol substrates (24). GOX catalyzes the oxidation of β -D-glucose to D-glucono- δ -lactone via a ping-pong steady-state kinetic mechanism in which oxygen reacts with ligand-free reduced enzyme (25). The active sites for sugar oxidation and oxygen reduction in GOX are both found above the *si*-face of the flavin ring. Klinman and Roth identified His516 as the site of oxygen activation in GOX and showed that the reaction requires the protonated form of this residue (2, 8, 9). His516 in GOX is hydrogen bonded to flavin N(5) via a bridging water molecule (Figure 1B), a feature similar to that observed for Lys265 in MSOX.

The pocket at the oxygen activation site, occupied by one or two water molecules in the observed crystal structures of MSOX and GOX, might provide a pre-organized binding site for superoxide anion during reaction of the reduced enzymes with oxygen. This scenario requires that oxygen displace at least one water molecule and occupy a polar reaction site. Nonpolar gases like xenon have traditionally been used to investigate oxygen-binding sites in nonpolar cavities (26–29). Chloride ion has been suggested as an alternate oxygen surrogate and used to probe recently discovered hydrophilic oxygen-binding sites in cofactor-less oxidases and oxygenases. Thus, chloride binds at the active site in urate oxidase, displacing a tightly hydrogen-bonded water molecule (30) (Figure 1C). A similar chloride-binding site is found in the formylglycine-generating enzyme (31) and

¹Abbreviations: FAD, flavin adenine dinucleotide, MSOX, monomeric sarcosine oxidase, GOX, glucose oxidase, MTA, methylthioacetate, RMSD, root-mean-squared deviation.

heteroaromatic oxygenases (32). Compelling evidence to show that oxygen and chloride bind at the same hydrophilic site in urate oxidase is provided by a crystal structure of the oxygen complex obtained under high oxygen pressure (4) (Figure 1D). Significantly, oxygen does not bind at a previously characterized xenon-binding site in urate oxidase.

In this paper we present biochemical and structural studies which show that chloride does indeed bind at the proposed sites of oxygen activation in MSOX and GOX.

EXPERIMENTAL PROCEDURES

Materials

Methylthioacetate was obtained from Sigma. Sarcosine was purchased from Isotec.

Enzyme Preparations

Wild-type MSOX and the Lys265Met MSOX mutant were prepared as previously described (6, 10, 33). GOX from *Aspergillus niger* was purchased from Sigma (G0543, 217 U/mg) and used for solution studies. For crystallization studies, GOX was partially deglycosylated by treatment with endoglycosidase H (New England Biolabs) and α -mannosidase (Sigma) as previously described (34).

Spectral Titrations

Absorption spectra were recorded using an Agilent Technologies 8453 diode array spectrophotometer. Dissociation constants for complexes formed with MSOX or GOX were determined by fitting a theoretical binding curve to absorbance changes at a given wavelength, as indicated in the text. Spectra corresponding to 100% complex formation were calculated as previously described (35).

Oxidative Half-reaction with Reduced MSOX

MSOX was reduced by reaction with 1 equivalent of sarcosine in anaerobic 50 mM potassium phosphate buffer, pH 8.0, containing 2.0 M potassium chloride. The kinetics of the reaction of the reduced enzyme with oxygen at 25 °C were monitored at 454 nm by using a Hi-Tech Scientific SF-62DX2 stopped-flow spectrophotometer in photomultipler mode, similar to that previously described (6). Reactions were initiated by mixing the reduced enzyme (1:1) with the same buffer saturated with oxygen/nitrogen gas mixtures containing 21.0, 44.0, 65.0 or 100.0% oxygen. Spectra of the reoxidized samples were recorded after each reaction. The absorption spectrum of the reduced enzyme was recorded after mixing with anaerobic buffer. Fitting of the kinetic traces was conducted using Sigma Plot 10 (Systat Software).

Crystallization of MSOX and Data collection

Crystals of ligand-free MSOX² were grown at 23° C from a solution containing 15 mg/ml protein and 1.9 M Na/K phosphate, pH 7.0 by the hanging drop method (using the Na/K phosphate in the reservoir) for about 1–2 weeks. To prepare the MSOX•chloride complex, crystals of ligand-free enzyme were soaked for 24 hours in 2.0 M Na/K phosphate, pH 7.0 and 2.5 M NaCl. For the reduced MSOX•sarcosine complex, ligand-free crystals were soaked in 2.0 M Na/K phosphate, pH 7.0 and 2.5 M NaCl for 24 h and then soaked in 2.0 M Na/K phosphate, pH 7.0, 2.3 M NaCl and 120 mM sarcosine for more than 1 h. To prepare

²Ligand-free MSOX refers to enzyme that does not contain any ligand at the sarcosine oxidation site or the oxygen activation site, as discussed in the text.

the MSOX•chloride•MTA complex, ligand-free crystals were soaked in 2.0 M Na/K phosphate, pH 7.0, 2.5 M NaCl and 12 mM MTA, each for about an hour.

For the MSOX•chloride complex crystal, X-ray data were recorded to 1.9 Å resolution from a single crystal soaked in Paraffin oil (Hampton Research) for 4 minutes at 100°K on an R axis IV image plate detector using a Rigaku RU200 X-ray generator using Cu K α radiation. For the MSOX•chloride•MTA complex and reduced MSOX•sarcosine complex crystals, X-ray data were recorded to 1.85 Å and 1.75 Å resolution, respectively, from single crystals also soaked in Paraffin oil for 4 minutes at 100°K, on a Quantum IV CCD detector at Beamline 14BMC of BIOCARS, APS, Argonne, IL. Data processing, indexing, integration, and scaling of the data were all performed with the HKL2000 package (36). All the crystals were monoclinic, space group P2₁ with two molecules per asymmetric unit with cell parameters a=70.9 Å, b=69.3 Å, c=72.9 Å, β=92.3° for the MSOX•chloride complex crystal, a=71.0 Å, b=69.5 Å, c=72.7 Å, β=92.3° for the reduced MSOX•sarcosine complex crystal and a=71.2 Å, b=69.7 Å, c=72.9 Å, β=92.3° for the MSOX•chloride•MTA complex crystal. The data collection statistics are summarized in Table 1.

Structure Refinement of MSOX Crystals

The structures of all three crystals were solved by molecular replacement with MOLREP from the ccp4 package (37) using the coordinates of subunit A from PDB ID code 2GBO, with all cofactors and solvent molecules omitted from the starting model. The refinement and electron density calculations were carried out using CNS (38) for the MSOX•chloride complex, the MSOX•chloride•MTA complex, and the reduced MSOX•sarcosine crystal; 5% of the reflections from each crystal were selected randomly and set aside as a test set for cross validation (39). Model building and analysis of the structure were carried out using COOT (40). Rigid body refinement before several cycles of positional and temperature factor refinement followed by interactive model building and automatic solvent placement with manual examination, were carried out. In the final stage of refinement, TLS tensors modeling rigid-body temperature factors were calculated and applied to the model. The final R_{cryst} and R_{free} were 0.184 and 0.212 for the MSOX•chloride complex crystal, 0.208 and 0.235 for the MSOX•chloride•MTA complex crystal and 0.184 and 0.217 for the reduced MSOX•sarcosine crystal, respectively. The refinement and model parameters are listed in Table 1.

Crystallization of GOX and Data collection

Crystals of partially deglycosylated GOX were grown in a solution containing 14 mg/ml protein plus 200 mM CaCl₂ and 20% PEG 3350 in 30 mM sodium phosphate pH 5.1 for crystal form A and 200 mM NaCl and 20% PEG 3350 in 30 mM sodium phosphate pH 5.1 for crystal form B by the hanging drop method at 22° C for about 2 weeks. Crystals for both crystal forms were cryoprotected in a solution similar to the mother liquid but containing 15% glycerol prior to flash freezing. X-ray diffraction data for both crystal form A and form B were collected on a Quantum IV CCD detector at Beamline 14BMC of BIOCARS, APS, Argonne, IL. Data processing, indexing, integration, and scaling were performed with the HKL2000 package (36). The crystals for form A were hexagonal, space group P3₁21 with unit cell parameters, a=b=65.9 Å, c=214.2 Å, and diffracted to 1.3 Å resolution. The crystals for form B were orthorhombic, space group C222₁ with unit cell parameters, a=69.6 Å, b=119.1 Å, c=142.2 Å, and diffracted to 1.2 Å resolution. There is one molecule per asymmetric unit for both crystal form A and form B. The data collection statistics are summarized in Supporting Information Table S1.

Structure Refinement of GOX Crystals

The structures of both GOX crystal forms were solved by molecular replacement with MOLREP from the ccp4 package (37) using the coordinates from PDB ID code 1CF3, with all solvent molecules omitted, as starting model. The refinement and electron density calculations for both structures were carried out using CNS (38) and 5% of the reflections were selected randomly and set aside as a test set for cross validation (39). Model building and analysis of both structures were carried out using COOT (40). Rigid body refinement before several cycles of positional and temperature factor refinement followed by interactive model building and automatic solvent placement with manual examination, were carried out. The final R_{cryst} and R_{free} were 0.180 and 0.198, and 0.178 and 0.188, with RMSD from ideal values of 0.014 Å and 0.012 Å for bond lengths and 1.6° and 1.6° for bond angles for crystal form A and form B, respectively. The refinement and model parameters are listed in Table S1.

Structural Calculation and Drawings

Structural diagrams were rendered using PYMOL (<http://www.pymol.org>).

RESULTS

Binding of Chloride to Ligand-free MSOX

The postulated binding of chloride at the oxygen activation site in MSOX will introduce a negative charge close to the flavin chromophore. Absorption spectra of flavoproteins are highly sensitive to changes in the local environment, suggesting that chloride binding might be detected by a perturbation of the visible absorption spectrum of MSOX. Ligand-free MSOX exhibits absorption maxima at 374 and 455 nm. Titration of the enzyme with chloride results in a dramatic 20-nm bathochromic shift of the near UV absorption maximum, accompanied by an increase in the intensity of this band, whereas the 455 nm absorption band is scarcely effected by chloride binding (Figure 2A). The corresponding difference spectra exhibit large negative and positive bands at 351 and 403 nm, respectively, plus smaller positive bands at 468 and 502 nm (Figure 2B). The dissociation constant for the MSOX•chloride complex was estimated based on the observed increase in absorbance at 404 nm ($K_d = 180 \pm 10$ mM) (Figure 2A, inset, Table 2). The chloride-induced spectral perturbation is not due to an ionic strength effect, as judged by control studies which show that the absorption spectrum of MSOX is unaffected by addition of 667 mM sodium sulfate or by increasing the phosphate buffer concentration from 50 to 785 mM, conditions that increase the ionic strength to a value equivalent to the addition of 2.0 M potassium chloride. Spectral perturbations are observed upon formation of MSOX complexes with carboxylic acid derivatives that resemble sarcosine and bind at the substrate oxidation site above the *re*-face of the flavin ring (11, 13). However, mutation of Lys265 to Met eliminates chloride binding, as judged by the fact that the absorption spectrum of the mutant is unaffected by addition of a high concentration of potassium chloride (2.0 M). This outcome is not expected nor observed with sarcosine analogs (6).

Does Chloride Affect the Binding of a Known Sarcosine Analog to MSOX?

We reasoned that the putative presence of chloride at the oxygen activation site should not block the binding of sarcosine analogs on the opposite face of the flavin ring. To evaluate this hypothesis, binding studies in the presence of excess chloride (2.0 M) were conducted using methylthioacetate (MTA, $\text{CH}_3\text{SCH}_2\text{CO}_2^-$), a sarcosine analog that forms a charge-transfer complex exhibiting a readily detectable absorption band in the long-wavelength region (11, 13). To control for a possible ionic strength effect, titrations of chloride-free enzyme with MTA were conducted in the presence or absence of an equivalent amount of

sulfate (667 mM), a divalent anion that does not bind to MSOX. Addition of MTA to the MSOX•chloride complex results in the development of an intense charge-transfer band (Figure 3A), as observed upon titration of ligand-free enzyme. The dissociation constant estimated for the binding of MTA to the MSOX•chloride complex ($K_d = 4.90 \pm 0.07$ mM) exhibits a modest 2- or 3-fold increase as compared with values observed for formation of the MSOX•MTA binary complex in the absence or presence of sulfate, respectively (Table 2). The charge-transfer band observed with the putative MSOX•chloride•MTA ternary complex ($\lambda_{max} = 528$ nm) exhibits a 4 nm hypsochromic shift as compared with that obtained for the binary MSOX•MTA complex in the absence or presence of sulfate ($\lambda_{max} = 532$ nm), as judged by the position of the bands observed in the corresponding difference spectra (Figure 3B). The results indicate that chloride and MTA occupy different binding sites and are consistent with the proposal that chloride binds at the oxygen activation site above the si-face of the flavin ring.

Binding of Chloride to GOX

Titration of GOX with chloride in 50 mM citrate buffer, pH 3.0, results in dramatic shifts in the position and intensity of absorption bands observed with the free enzyme at 383 and 453 nm. Formation of the GOX•chloride complex causes a pronounced hypsochromic shift (14 nm) and increase in the intensity of the near UV band whereas the 453 nm band undergoes a substantial bathochromic shift (13 nm) and a decrease in intensity (Figure 4A). Consequently, the two absorption maxima at $\lambda > 300$ nm are much further apart (27 nm) in the GOX•chloride complex as compared with the free enzyme. The opposite scenario is observed with MSOX where the maxima are much closer (20 nm) in the chloride complex. Difference spectra calculated for the titration of GOX with chloride exhibit prominent positive peaks at 360 and 504 nm and a broad negative peak centered at ~425 with pronounced shoulders at 402 and 446 nm (Figure 4B). The dissociation constant for the GOX•chloride complex at pH 3.0 ($K_d = 6.2 \pm 0.1$ mM) was determined by analysis of the observed increase in absorbance at 504 nm (Figure 4A, inset).

A 1000-fold greater reactivity of the reduced enzyme with oxygen is observed upon protonation of His516, the site of oxygen activation in GOX (8). We reasoned that a similar pH-dependence should be observed for chloride binding, assuming that the halide binds at the oxygen activation site in GOX. To test this hypothesis, chloride titrations with GOX were conducted in the pH range from 3.0 to 7.0. The spectral perturbations observed at higher pH values are very similar to that observed at pH 3.0 (data not shown). A pronounced decrease in the stability of the GOX•chloride complex is, however, seen at pH values above 3 (data not shown; see Table S2 in Supporting Information). Analysis of the effect of pH on chloride binding indicates that a ~400-fold decrease in complex stability occurs upon deprotonation of a group with a pK_a of 6.20 ± 0.05 (Figure 5). The observed pK_a is similar to that obtained with free histidine ($pK_a = 6.0$) but lower than reported for His516 in reduced GOX ($pK_a = 8.1$) (8). The perturbed pK_a value of His516 in the reduced enzyme is attributable to electrostatic stabilization of the protonated imidazole by the nearby reduced flavin anion.

Attempt to Prepare Crystals of the Binary GOX•Chloride Complex

GOX was crystallized from 20% PEG3350 in 30 mM sodium phosphate, pH 5.1, containing 200 mM CaCl₂ or 200 mM NaCl to yield crystals (A or B) that diffracted to a higher resolution (1.3 or 1.2 Å, respectively) compared to crystals previously obtained under different conditions (1CF3.pdb, 1.9 Å resolution) (23, 41). Crystal A belongs to same space group (P3₁21) as 1CF3.pdb whereas crystal B exhibits a new lattice (C222₁)3 (data not

³Comparison of the GOX molecule in crystal A or B with that in 1CF3.pdb shows an RMSD of 0.28 or 0.39 Å, respectively.

shown; see Table S1 in Supporting Information). Crystals A and B were produced at a chloride concentration similar to the dissociation constant observed for formation of the GOX•chloride complex in solution at pH 5. However, neither crystal contained chloride at the active site⁴, suggesting that the stability of the chloride complex may have been adversely affected by the presence of PEG in the crystallization buffer. In a further attempt to prepare the crystalline complex, the GOX crystals were soaked under conditions known to promote formation of the enzyme•chloride complex in solution (2.5 M NaCl in 100 mM sodium acetate, pH 4.5). However, the crystals dissolved after 2 h under these conditions.

Crystal Structure of the Binary MSOX•Chloride Complex

To grow crystals of ligand-free MSOX2, equal volumes of protein (in 20 mM Tris-HCl, pH 8.0) and reservoir (1.9 M Na/K phosphate, pH 7.0) solutions were mixed and allowed to equilibrate. The ligand-free crystals were soaked in phosphate buffer containing 2.5 M sodium chloride to produce crystals of the MSOX•chloride complex. This complex contains a chloride ion above the *si*-face of the flavin ring in each of the two molecules in the asymmetric unit. The chloride is bound at nearly the same position occupied by WAT2 in ligand-free enzyme. The bound chloride forms hydrogen bonds to Lys265:NZ (2.99 Å), Arg49:NH1 (3.14 Å), WAT1 (3.17 Å), and WAT3 (3.11 Å) (Figure 6, top panel). The average B-factors for chloride, WAT1 and WAT3 are 26, 20 and 27 Å², respectively. WAT3 is not detected in ligand-free MSOX or the MSOX•MTA complex but is found in some complexes with other sarcosine analogs (Table 3, footnote f). Binding of chloride above the *si*-face of the flavin ring does not significantly perturb the region above the *re*-face of the flavin with the notable exception of Glu57 and Arg 52 (Figure 6, bottom panel). Glu57 is part of a loop (Tyr55-Tyr61) that controls access to the sarcosine oxidation active site. This loop is in a closed configuration in both molecules of the asymmetric unit in crystals of the chloride complex. The same loop configuration is observed in complexes of MSOX with sarcosine analogs. In contrast, the loop is mobile in ligand-free MSOX, as judged by the open and closed configurations observed in molecules 1 and 2, respectively (Table 3). Arg52 is found in the “in” position in the chloride complex and in MSOX complexes with sarcosine analogs where the residue binds the carboxylate moiety of the substrate analog. In contrast, Arg52 is mainly in the “out” position in ligand-free MSOX (Table 3). Except for minor variations in an external loop, no significant difference in backbone structure is detected upon comparison of the chloride complex with chloride-free MSOX, as judged by RMSD values (Table 3).

It should be noted MSOX contains a second chloride binding site near the ribityl moiety of FAD. The chloride at the second site is bound by four ligands: FAD:O3* (3.10 Å), Gly344:N (3.11 Å), Thr318:N (3.34 Å), and a water (3.03 Å). The geometry is more nearly square planar. The chloride at the second site is more tightly bound (average B-factor = 17 Å²) than the chloride at the *si*-face binding site, and is found in all MSOX crystals.

Crystal Structure of the MSOX•Chloride•MTA Ternary Complex

Crystals of the MSOX•chloride•MTA complex were generated by soaking ligand-free crystals in phosphate buffer containing sodium chloride and MTA (12 mM). Chloride is bound above the *si*-face of the flavin ring in the ternary complex at nearly the same position occupied by WAT2 in the MSOX•MTA binary complex (Figure 7, top panel) or ligand-free enzyme. The same four ligands bind chloride in the ternary complex as observed for chloride in the binary MSOX•chloride complex. MTA is bound above the *re*-face of the flavin in the ternary complex. The active site loop that controls access to the *re*-face is in the

⁴Both crystalline forms of GOX contain a chloride ion at the surface of the protein that is hydrogen bonded to 3 or 4 water molecules and Glu221:N.

closed configuration. Arg52 is in the “in” position and forms hydrogen bonds to the carboxylate of MTA which is also hydrogen bonded to Lys348:NZ. The region above the *re*-face of the flavin in the ternary complex is virtually identical to that observed in the binary MSOX•MTA complex (Figure 7, bottom panel). The two complexes also exhibit nearly identical backbone structures, as judged by RMSD values (Table 3). The crystal structure of the ternary complex provides compelling evidence in support of deductions made based on results obtained by spectrophotometric titration in solutions studies.

Crystal Structure of the reduced MSOX•Sarcosine Complex and Related Biochemical Studies

Crystals of ligand-free MSOX were soaked in phosphate buffer containing NaCl and sarcosine (120 mM). The sarcosine soak results in enzyme reduction, as judged by the bleaching of the bright yellow color of the starting crystals of oxidized MSOX. A ligand is bound above the *re*-face of the reduced flavin ring which retains the nearly planar configuration observed with oxidized enzyme. It is not possible to distinguish between sarcosine and its imine at 1.75 Å resolution. However, the imine in the initially formed reduced enzyme•product complex is likely to be displaced by sarcosine, present in large excess in the soaking solution. On this basis, the ligand in the reduced crystal is modeled as sarcosine. The active site loop is in the closed conformation and Arg52 is in the “in” position (Table 3). The ligand carboxylate forms hydrogen bonds to Arg52 and Lys348. The ligand amino group is hydrogen bonded to the carbonyl oxygen of Gly344. The ligand binding mode and conformation of residues above the *re*-face in the reduced enzyme•sarcosine complex are virtually identical to that observed for a complex of the oxidized MSOX with dimethylglycine (DMG), a sarcosine (N-methylglycine) analog that acts as a competitive inhibitor (Figure 8, bottom panel). Although the reduced enzyme•sarcosine complex was produced in the presence of a high concentration of chloride, the crystals of this complex contain WAT2 above the *si*-face of the flavin (Figure 8, top panel) instead of the chloride ion found at this position in the binary and ternary complexes with oxidized MSOX, as described above.

The results indicate that the apparent stability of the crystalline chloride complex is greatly decreased upon enzyme reduction. To determine whether a similar phenomenon occurs in solution, we investigated the effect of a high concentration of chloride (2.0 M) on the reaction of the reduced enzyme with oxygen. We reasoned that the reaction should be strongly inhibited if chloride is bound at the oxygen activation site under these conditions. This outcome is, however, contrary to that predicted based on the observed crystal structure of reduced MSOX. In fact, the oxidative half-reaction is very fast in the presence of 2.0 M chloride and was monitored by using a stopped-flow spectrophotometer. A monophasic exponential increase in absorbance at 454 nm is observed at various oxygen concentrations (Figure 9A). The observed rate constants are directly proportional to the oxygen concentration (Figure 9B). The second-order rate constant determined from the slope of this plot ($k = 2.48 \pm 0.03 \times 10^5 \text{ M}^{-1} \text{ s}^{-1}$) is virtually identical to a value previously determined for the reaction in the absence of chloride ($k = 2.83 \pm 0.07 \times 10^5 \text{ M}^{-1} \text{ s}^{-1}$) (6). The kinetic data indicate that chloride is not bound at the oxygen activation site in solutions of reduced MSOX containing a high concentration of chloride. Consistent with the kinetic data, chloride does not perturb the absorption spectrum of reduced MSOX. However, absorption spectra recorded at the end of each oxidative half-reaction show that the reoxidized enzyme readily binds chloride under these conditions (Figure 9A, inset).

DISCUSSION

GOX contains a single active site for sugar oxidation and oxygen reduction above the *si*-face of the flavin ring and catalyzes the oxidation of glucose via a ping-pong mechanism (25).

MSOX contains separate active sites for amino acid oxidation and oxygen reduction above the *re*-and *si*-faces of the flavin ring, respectively, and catalyzes sarcosine oxidation via a ternary complex mechanism in which oxygen reacts with a reduced enzyme•sarcosine imine complex (12). A single positively charged residue, His516 or Lys265, is the site of oxygen activation in GOX or MSOX, respectively, and solely responsible for the enormous rate accelerations observed with the wild-type enzymes (2, 6–9). Crystal structures of GOX and MSOX display a small pocket, containing one or two water molecules, at the oxygen activation site that could serve as a pre-organized binding site for superoxide anion, an obligatory initial intermediate in the 2-electron reduction of oxygen (see Scheme 1).

Results obtained in solution studies strongly suggest that chloride binds at the oxygen activation site in GOX and MSOX. Thus, both enzymes form spectrally detectable complexes with chloride. Tight binding of chloride to oxidized GOX requires protonation of a residue that exhibits a pK_a value similar to that observed for free histidine. The protonated form of His516 is required for the rapid reaction of reduced GOX with oxygen. The results strongly suggest that the protonated form of same active site histidine is also required for chloride binding. Formation of a binary MSOX•chloride complex requires Lys265 and is blocked upon replacing this lysine with a neutral residue. Binding of chloride to MSOX does not affect the binding of MTA, a sarcosine analog that binds above the *re*-face of the flavin ring. Definitive evidence for the proposed chloride binding site is provided by crystal structures determined for a binary MSOX•chloride complex and a ternary MSOX•chloride•MTA complex. In each case, chloride is bound in the small pocket above the *si*-face of the flavin ring at a position otherwise occupied by an active site water (WAT2) that is hydrogen bonded to Lys265 in free MSOX or the MSOX•MTA binary complex. MSOX-bound chloride forms hydrogen bonds with Lys265:NZ, Arg49:NH1 and two water molecules, one of which is also hydrogen bonded to FAD:N5. The arrangement of the four chloride ligands exhibits approximate tetrahedral geometry.

The results show that chloride can act as a surrogate for oxygen in two flavoprotein oxidases, similar to that observed with urate oxidase and other cofactor-less oxidases (30–32). It is noteworthy that a chloride ion is found close to FAD:N(5) in a crystal structure of vanillyl alcohol oxidase, forming hydrogen bonds to two backbone amide nitrogens in an oxyanion-like hole (42). It has been suggested that the chloride-binding site may be the site of oxygen activation in vanillyl alcohol oxidase (43). In this scenario, the dipoles of two peptide nitrogen atoms create a pre-organized superoxide anion binding site, analogous to that achieved by a single basic residue in GOX or MSOX. Overall, the results with various oxidases indicate that chloride is an effective probe of polar oxygen activation sites, providing a valuable complementary tool to the xenon gas method that has been used to map nonpolar oxygen-binding cavities (26–29). Of course, like xenon, chloride is also promiscuous and can bind to sites in enzymes unrelated to oxygen activation, as illustrated by the second chloride binding site in MSOX near the ribityl side chain of FAD. Another example is provided by members of the Old Yellow Enzyme family where chloride is bound by a pair of histidines in an anion-binding cavity that otherwise stabilizes the development of a negative charge in α,β -unsaturated carbonyl substrates during hydride transfer from reduced flavin (44). The above examples stress the importance of cross-validation through experimental verification in using chloride as a potential oxygen surrogate.

The steady-state kinetic mechanism observed for MSOX (12), in conjunction with the generally accepted mechanism for oxygen reduction (see Scheme 1), strongly suggest that a ternary complex will be produced during aerobic turnover of MSOX that contains a neutral flavin radical, superoxide anion, and sarcosine imine (Scheme 2). The best available structural model for this reactive intermediate is provided by the crystal structure obtained for the MSOX•chloride•MTA ternary complex. The second-order kinetics observed for the

reaction of reduced MSOX with oxygen are consistent with a simple bimolecular reaction. However, the results do not rule out reaction via a Michaelis complex, containing a reduced FAD anion (FADH^-), molecular oxygen and sarcosine imine (Scheme 2), that is unstable ($K_d = 10 \text{ mM}$) and therefore difficult to detect within the accessible range of oxygen concentrations. We hoped to generate a model for this 2-electron reduced enzyme ternary complex by using chloride and MTA as surrogates for oxygen and sarcosine imine, respectively. Structural and kinetic data, however, indicate that reduction of MSOX results in a large decrease in chloride binding affinity, compared with oxidized MSOX ($K_d = 180 \text{ mM}$, pH 8.0)⁵. This outcome is attributed to electrostatic repulsion between the halide ion and the negative charge of the adjacent anionic reduced flavin. A similar effect is observed with pentaerythritol tetranitrate reductase, a member of the Old Yellow Enzyme family, where chloride binding is observed with oxidized but not reduced enzyme (44). Importantly, the negative charge of the reduced flavin anion is lost upon 1-electron reduction of oxygen and, consequently, will not adversely affect the proposed binding of superoxide anion in the pocket occupied by chloride in complexes with oxidized MSOX.

Supplementary Material

Refer to Web version on PubMed Central for supplementary material.

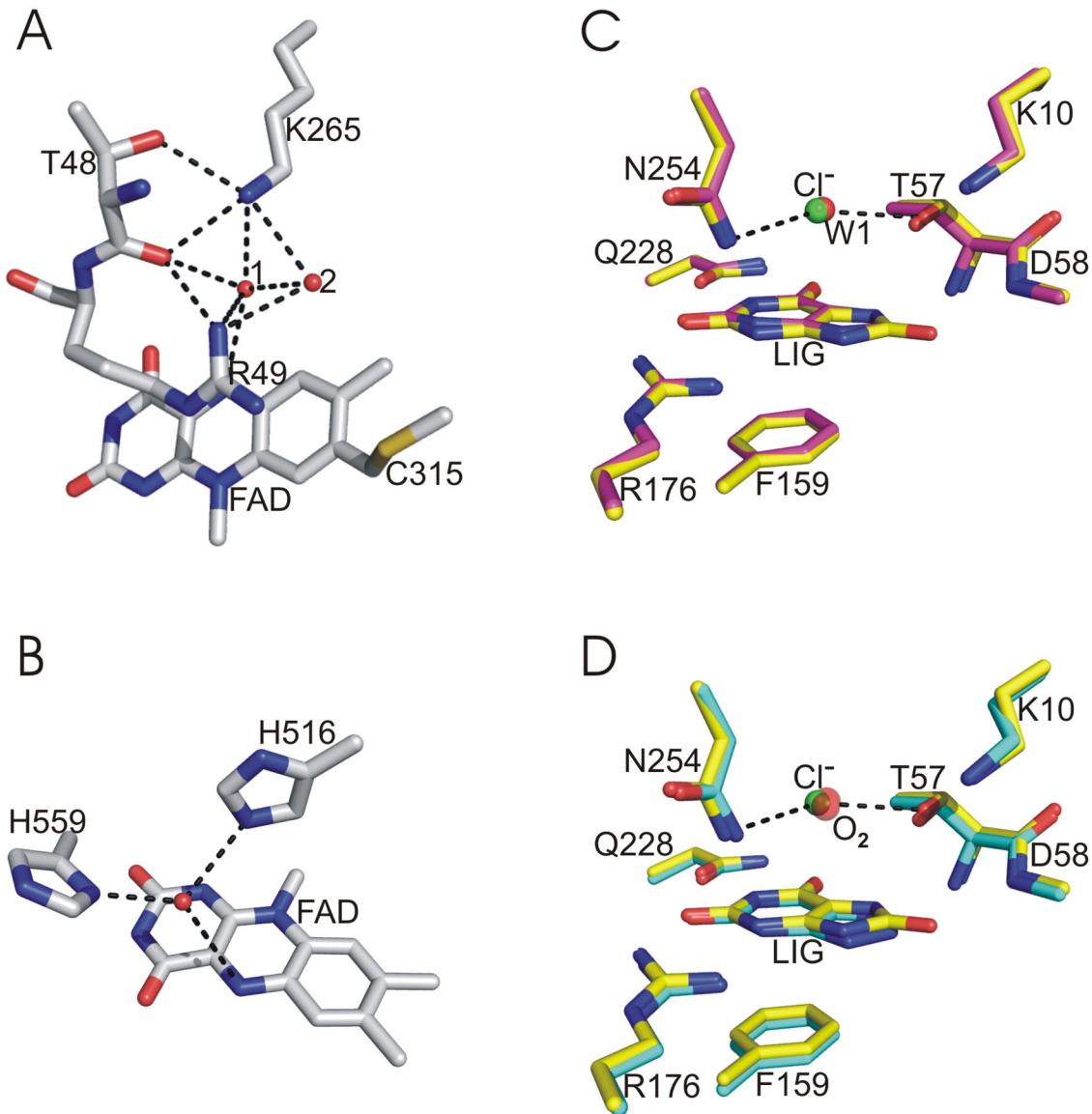
References

1. Massey V. Activation of molecular oxygen by flavins and flavoproteins. *J Biol Chem.* 1994; 269:22459–22462. [PubMed: 8077188]
2. Klinman JP. How do enzymes activate oxygen without inactivating themselves? *Acc Chem Res.* 2007; 40:325–333. [PubMed: 17474709]
3. Sucharitakul J, Prongkit M, Haltrich D, Chaiyen P. Detection of a C4a-hydroperoxyflavin intermediate in the reaction of a flavoprotein oxidase. *Biochemistry.* 2008; 47:8485–8490. [PubMed: 18652479]
4. Colloc'h N, Gabison L, Monard G, Altarsha M, Chiadmi M, Marassio G, Santos JSDO, El Hajji M, Castro B, Abraimai JH, Prange T. Oxygen pressurized X-ray crystallography: Probing the dioxygen binding site in cofactorless urate oxidase and implications for its catalytic mechanism. *Biophys J.* 2008; 95:2415–2422. [PubMed: 18375516]
5. Lind J, Shen X, Merenyi G, Jonsson BO. Determination of the rate constant of self-exchange of the $\text{O}_2/\text{O}_2^\bullet$ - couple in water by $^{18}\text{O}/^{16}\text{O}$ isotope marking. *J Am Chem Soc.* 1989; 111:7654–7655.
6. Zhao G, Bruckner RC, Jorns MS. Identification of the oxygen activation site in monomeric sarcosine oxidase: Role of Lys265 in catalysis. *Biochemistry.* 2008; 47:9124–9135. [PubMed: 18693755]
7. Jorns MS, Chen Z, Mathews FS. Structural characterization of mutations at the oxygen activation site in monomeric sarcosine oxidase. *Biochemistry.* 2010; 49:3631–3639. [PubMed: 20353187]
8. Roth JP, Klinman JP. Catalysis of electron transfer during activation of O_2 by the flavoprotein glucose oxidase. *Proc Natl Acad Sci USA.* 2003; 100:62–67. [PubMed: 12506204]
9. Roth JP, Wincek R, Nodet G, Edmondson DE, McIntire WS, Klinman JP. Oxygen isotope effects on electron transfer to O_2 probed using chemically modified flavins bound to glucose oxidase. *J Am Chem Soc.* 2004; 126:15120–15131. [PubMed: 15548009]
10. Wagner MA, Khanna P, Jorns MS. Structure of the flavocoenzyme of two homologous amine oxidases: Monomeric sarcosine oxidase and N-methyltryptophan oxidase. *Biochemistry.* 1999; 38:5588–5595. [PubMed: 10220347]

⁵A 30-fold higher affinity for chloride is observed with oxidized GOX at acidic pH ($K_d = 6.2 \text{ mM}$, pH 3.0). This suggested that we might detect the formation of an inhibitory reduced GOX•chloride complex by monitoring the reaction of reduced GOX with oxygen in the presence of a high concentration of chloride. This hypothesis could not, however, be tested because solutions of GOX are stable at pH 3.0 only in the presence of modest concentrations of chloride (< 50 mM NaCl).

11. Trickey P, Wagner MA, Jorns MS, Mathews FS. Monomeric sarcosine oxidase: Structure of a covalently-flavinylated secondary amine oxidizing enzyme. *Structure*. 1999; 7:331–345. [PubMed: 10368302]
12. Wagner MA, Jorns MS. Monomeric sarcosine oxidase: 2. Kinetic studies with sarcosine, alternate substrates and substrate analogs. *Biochemistry*. 2000; 39:8825–8829. [PubMed: 10913293]
13. Wagner MA, Trickey P, Chen Z, Mathews FS, Jorns MS. Monomeric sarcosine oxidase: 1. Flavin reactivity and active site binding determinants. *Biochemistry*. 2000; 39:8813–8824. [PubMed: 10913292]
14. Fossati P, Prencipe L, Berti G. Enzymic creatinine assay: A new colorimetric method based on hydrogen peroxide measurement. *Clin Chem*. 1983; 29:1494–1496. [PubMed: 6872208]
15. Berberich JA, Yang LW, Madura J, Bahar I, Russell AJ. A stable three-enzyme creatinine biosensor. 1 Impact of structure, function and environment on PEGylated and immobilized sarcosine oxidase. *Acta Biomaterialia*. 2005; 1:173–181. [PubMed: 16701794]
16. Khanna P, Jorns MS. Characterization of the FAD-containing N-methyltryptophan oxidase from *Escherichia coli*. *Biochemistry*. 2001; 40:1441–1450. [PubMed: 11170472]
17. Venci D, Zhao G, Jorns MS. Molecular characterization of nikD, a new flavoenzyme important in the biosynthesis of nikkomycin antibiotics. *Biochemistry*. 2002; 41:15795–15802. [PubMed: 12501208]
18. Wu XL, Takahashi M, Chen SG, Monnier VM. Cloning of amadoriase I isoenzyme from *Aspergillus sp.*: Evidence of FAD covalently linked to Cys342. *Biochemistry*. 2000; 39:1515–1521. [PubMed: 10684633]
19. Dodt G, Kim DG, Reimann SA, Reuber BE, McCabe K, Gould SJ, Mihalik SJ. L-pipecolic acid oxidase, a human enzyme essential for the degradation of L-pipecolic acid, is most similar to the monomeric sarcosine oxidases. *Biochem J*. 2000; 345:487–494. [PubMed: 10642506]
20. Kohen A, Jonsson T, Klinman JP. Effect of protein glycosylation on catalysis: Changes in hydrogen tunneling and enthalpy of activation in the glucose oxidase reaction. *Biochemistry*. 1997; 36:2603–2611. [PubMed: 9054567]
21. Swoboda BEP, Massey V. Purification and properties of the glucose oxidase from *Aspergillus niger*. *J Biol Chem*. 1965; 240:2209–2215. [PubMed: 14299649]
22. Hecht HJ, Kalisz HM, Hendle J, Schmid RD, Schomburg D. Crystal structure of glucose oxidase from *Aspergillus niger* refined at 2.3 angstrom resolution. *J Mol Biol*. 1993; 229:153–172. [PubMed: 8421298]
23. Wohlfahrt G, Witt S, Hendle J, Schomburg D, Kalisz HM, Hecht HJ. 1.8 and 1.9 angstrom resolution structures of the *Penicillium amagasakiense* and *Aspergillus niger* glucose oxidases as a basis for modelling substrate complexes. *Acta Crystallogr Sect D*. 1999; 55:969–977. [PubMed: 10216293]
24. Cavener DR. GMC oxidoreductases: A newly defined family of homologous proteins with diverse catalytic activities. *J Mol Biol*. 1992; 223:811–814. [PubMed: 1542121]
25. Gibson QH, Swoboda BEP, Massey V. Kinetics and mechanism of action of glucose oxidase. *J Biol Chem*. 1964; 239:3927–3934. [PubMed: 14257628]
26. Cohen J, Arkhipov A, Braun R, Schulten K. Imaging the migration pathways for O₂, CO, NO, and Xe inside myoglobin. *Biophys J*. 2006; 91:1844–1857. [PubMed: 16751246]
27. Duff AP, Trambaiolo DM, Cohen AE, Ellis PJ, Juda GA, Shepard EM, Langley DB, Dooley DM, Freeman HC, Guss JM. Using xenon as a probe for dioxygen-binding sites in copper amine oxidases. *J Mol Biol*. 2004; 344:599–607. [PubMed: 15533431]
28. Hiromoto T, Fujiwara S, Hosokawa K, Yamaguchi H. Crystal structure of 3-hydroxybenzoate hydroxylase from *Comamonas testosteroni* has a large tunnel for substrate and oxygen access to the active site. *J Mol Biol*. 2006; 364:878–896. [PubMed: 17045293]
29. Wade RC, Winn PJ, Schlichting I, Sudarko PJ. A survey of active site access channels in cytochromes P450. *J Inorg Biochem*. 2004; 98:1175–1182. [PubMed: 15219983]
30. Gabison L, Chiadmi M, El Hajji M, Castro B, Colloc'h N, Prange T. Near-atomic resolution structures of urate oxidase complexed with its substrate and analogues: the protonation state of the ligand. *Acta Crystallogr Sect D*. 2010; 66:714–724. [PubMed: 20516624]

31. Roeser D, Schmidt B, Preusser-Kunze A, Rudolph MG. Probing the oxygen-binding site of the human formylglycine-generating enzyme using halide ions. *Acta Crystallogr Sect D*. 2007; 63:621–627. [PubMed: 17452787]
32. Steiner RA, Janssen HJ, Roversi P, Oakley AJ, Fetzner S. Structural basis for cofactor-independent dioxygenation of N-heteroaromatic compounds at the α/β -hydroxylase fold. *Proc Natl Acad Sci USA*. 2010; 107:657–662. [PubMed: 20080731]
33. Hassan-Abdallah A, Bruckner RC, Zhao G, Jorns MS. Biosynthesis of covalently bound flavin: Isolation and in vitro flavinylation of the monomeric sarcosine oxidase apoprotein. *Biochemistry*. 2005; 44:6452–6462. [PubMed: 15850379]
34. Courjean O, Gao F, Mano N. Deglycosylation of glucose oxidase for direct and efficient glucose electrooxidation on a glassy carbon electrode. *Angew Chem Int Ed*. 2009; 48:5897–5899.
35. Zhao G, Jorns MS. Spectral and kinetic characterization of the Michaelis charge transfer complex in monomeric sarcosine oxidase. *Biochemistry*. 2006; 45:5985–5992. [PubMed: 16681370]
36. Otwinowski Z, Minor W. Processing of X-ray diffraction data collected in oscillation mode. *Methods Enzymol*. 1997; 276:307–326.
37. CCP4. Collaborative Computational Project Number 4. *Acta Crystallogr Sect D*. 1994; 50:760–763. [PubMed: 15299374]
38. Brünger AT, Adams PD, Clore GM, DeLano WL, Gros P, Grosse-Kunstleve RW, Jiang JS, Kuszewski J, Nilges M, Pannu NS, Read RJ, Rice LM, Simonson T, Warren GL. Crystallography & NMR system: A new software suite for macromolecular structure determination. *Acta Crystallogr Sect D*. 1998; 54:905–921. [PubMed: 9757107]
39. Kleywegt GJ, Brünger AT. Checking your imagination: Application of the free r value. *Structure*. 1996; 4:897–904. [PubMed: 8805582]
40. Emsley P, Cowtan K. Coot: Model-building tools for molecular graphics. *Acta Crystallogr Sect D*. 2004; 60:2126–2132. [PubMed: 15572765]
41. Kalisz HM, Hecht HJ, Schomburg D, Schmid RD. Crystallization and preliminary X-ray diffraction studies of a deglycosylated glucose oxidase from *Aspergillus niger*. *J Mol Biol*. 1990; 213:207–209. [PubMed: 2342102]
42. Mattevi A, Fraaije MW, Mozzarelli A, Olivi L, Coda A, Vanberkel WJH. Crystal structures and inhibitor binding in the octameric flavoenzyme vanillyl-alcohol oxidase; The shape of the active site cavity controls substrate specificity. *Structure*. 1997; 5:907–920. [PubMed: 9261083]
43. Mattevi A. To be or not to be an oxidase: challenging the oxygen reactivity of flavoenzymes. *TIBS*. 2006; 31:276–283. [PubMed: 16600599]
44. Barna TM, Khan H, Bruce NC, Barsukov I, Scrutton NS, Moody PCE. Crystal structure of pentaerythritol tetranitrate reductase: “Flipped” binding geometries for steroid substrates in different redox states of the enzyme. *J Mol Biol*. 2001; 310:433–447. [PubMed: 11428899]
45. Zhao G, Song H, Chen Z, Mathews FS, Jorns MS. Monomeric sarcosine oxidase: Role of histidine 269 in catalysis. *Biochemistry*. 2002; 41:9751–9764. [PubMed: 12146941]

**Figure 1.**

Oxygen activation sites in MSOX, GOX and urate oxidase. In each panel, carbon atoms are colored as indicated, oxygen atoms are red, nitrogen atoms are blue, sulfur is yellow, and chloride is green. Hydrogen bonds are indicated by dashed lines. Panel A: Region above the *si*-face of the flavin ring in MSOX (white carbons) (PDB code 2GBO); Panel B: Region above the *re*-face of the flavin ring in glucose oxidase (white carbons) (PDB code 1CF3). Panel C: Comparison of the urate oxidase•chloride•urate ternary complex (yellow carbons) (PDB code 3L9G) with the urate oxidase•xanthine binary complex (magenta carbons) (PDB code 3L8W). Panel D: Comparison of the urate oxidase•chloride•urate ternary complex (yellow carbons) (PDB code 3L9G) with the urate oxidase•oxygen•azaxanthine complex (cyan carbons) (PDB code 2ZKA.pdb)

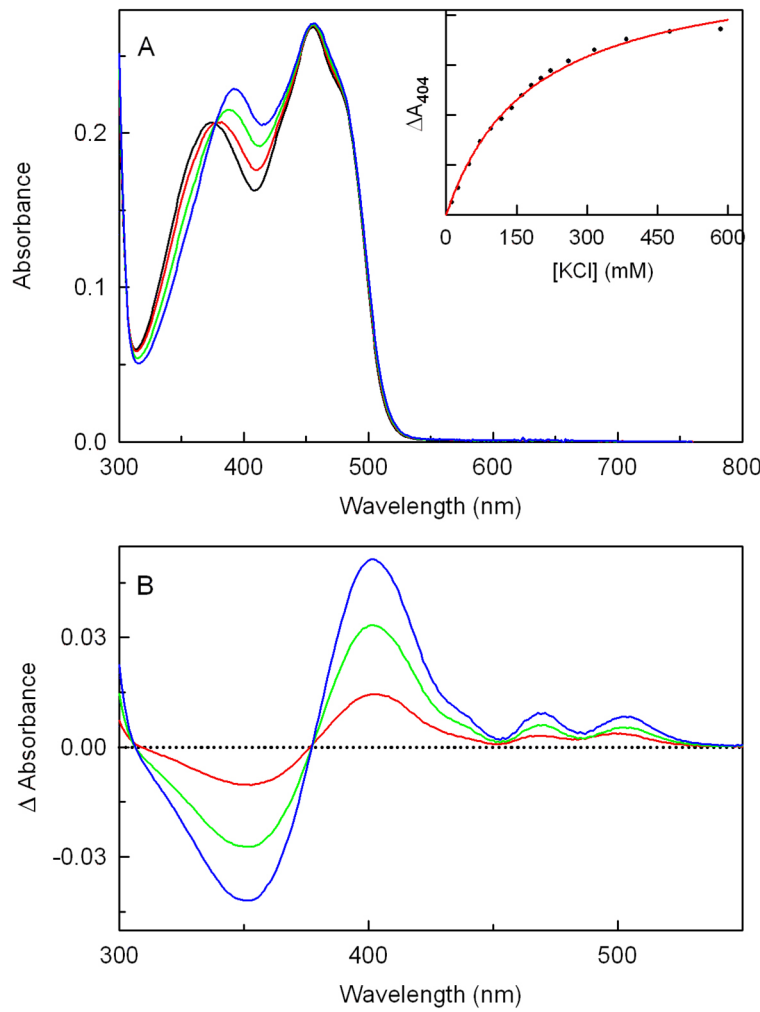
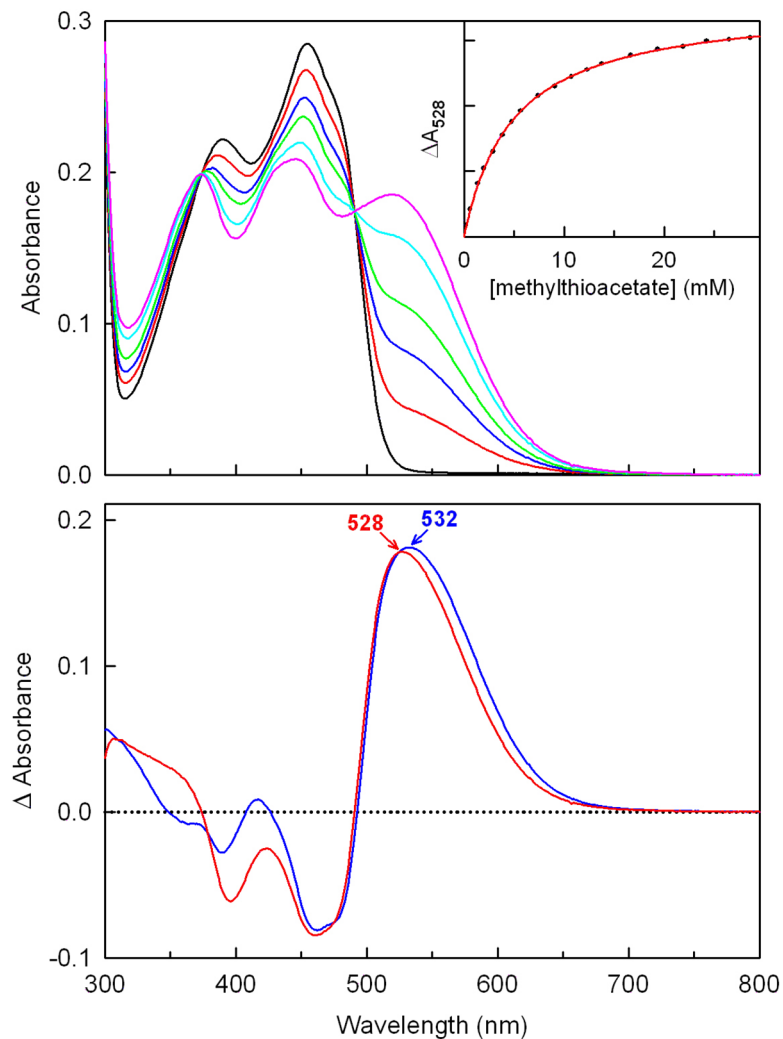
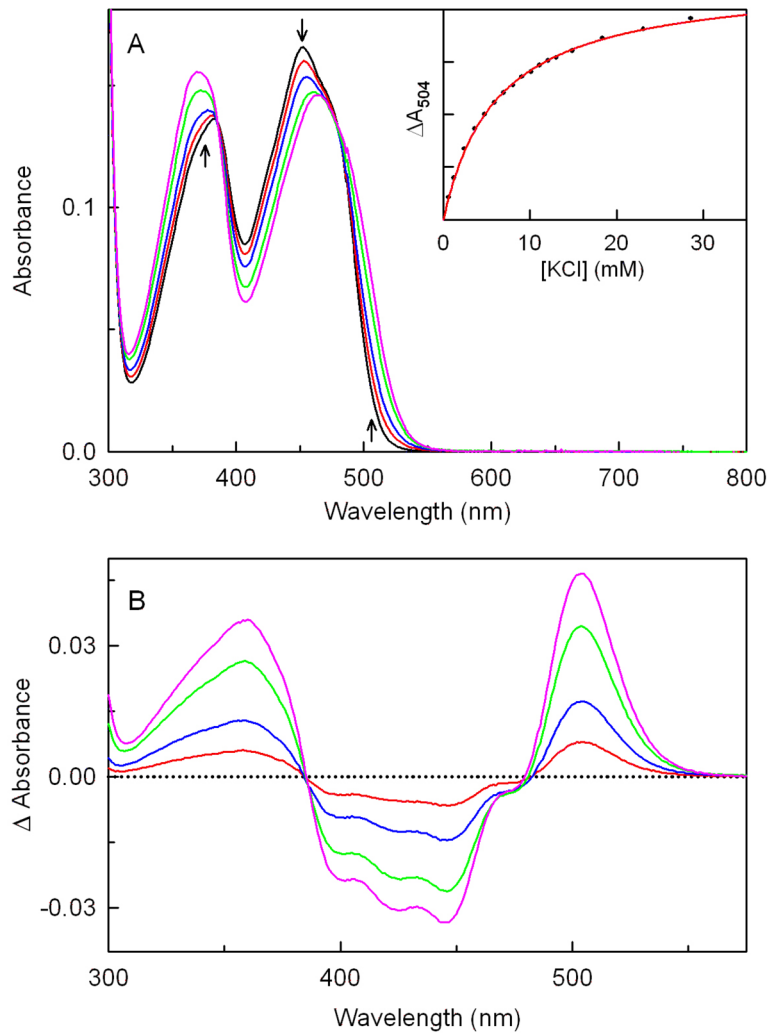


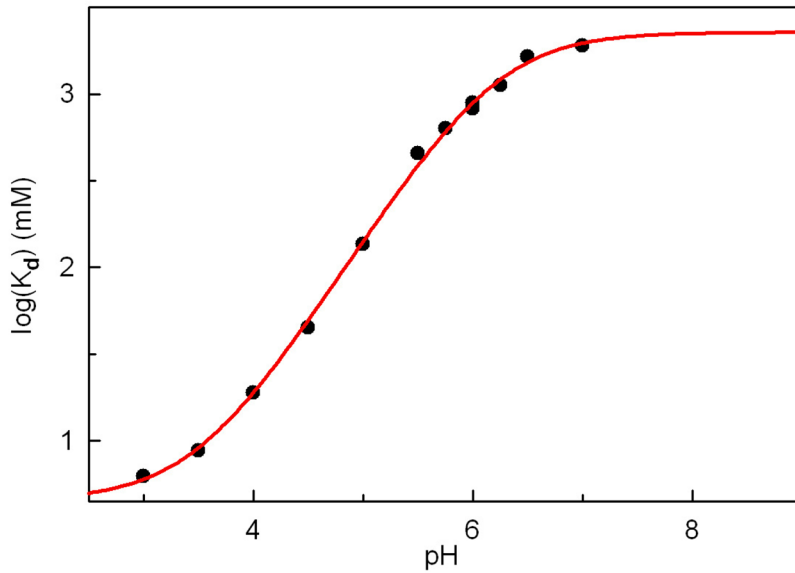
Figure 2. Spectral properties of the binary complex formed with MSOX and chloride. The spectral titration was conducted in 50 mM potassium phosphate buffer, pH 8.0, at 25 °C. Panel A: Absorption spectra recorded in the presence of 0, 72.3 and 315.8 mM potassium chloride are shown in the black, red and green curves, respectively. The blue curve is the absorption spectrum calculated for 100% complex formation, as described in Experimental Procedures. The inset shows a plot of absorbance changes at 404 nm as a function of the concentration of chloride. The solid red line was obtained by fitting a theoretical binding curve ($\Delta A_{\text{obs}} = \Delta A_{\text{max}}[\text{ligand}]/(K_d + [\text{ligand}])$) to the data (black circles). Panel B shows the corresponding difference spectra obtained by subtracting the spectrum of free MSOX from spectra observed in the presence of chloride.

**Figure 3.**

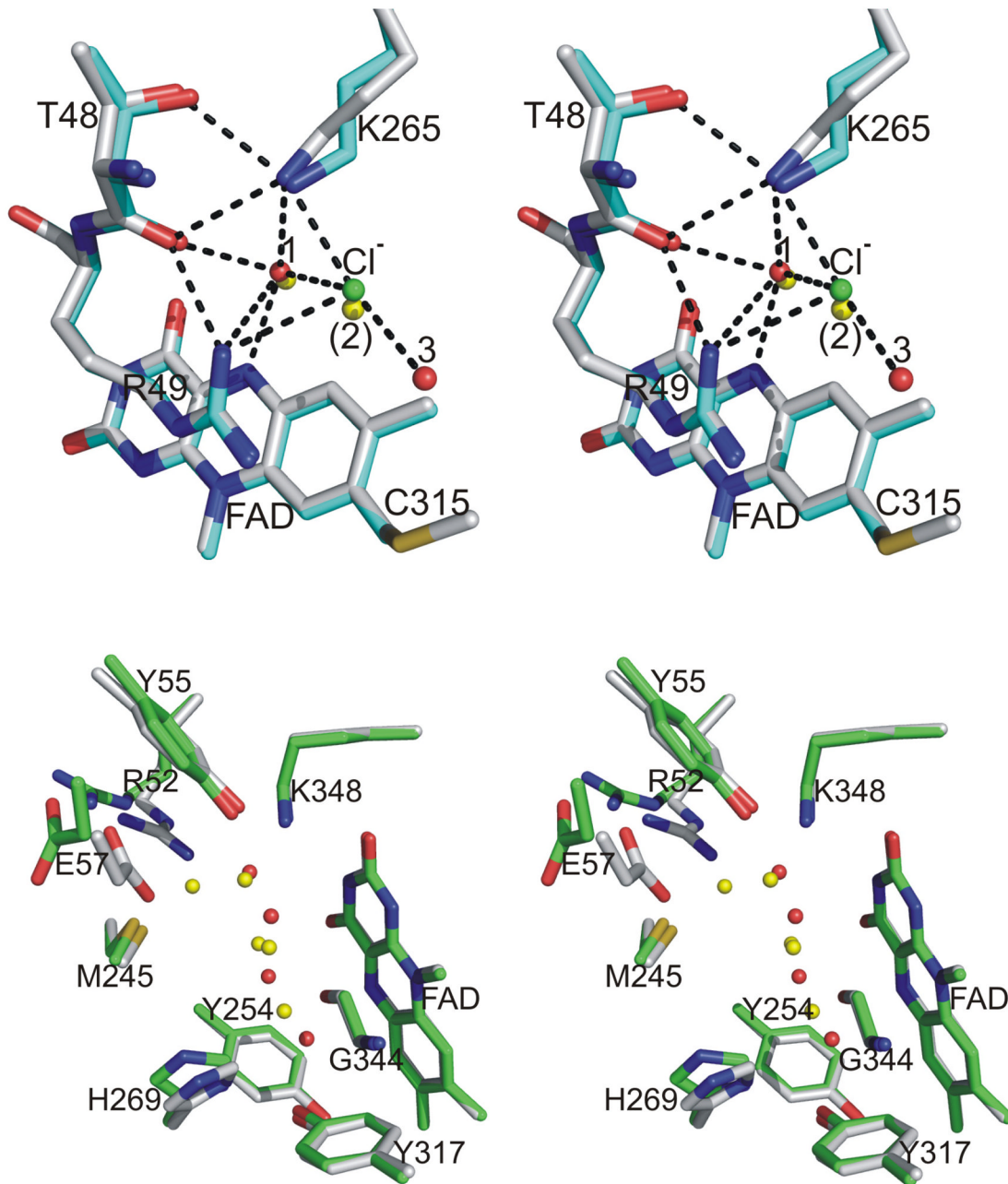
Titration of the MSOX•chloride binary complex with methylthioacetate (MTA). Panel A: The absorption spectrum of the MSOX•chloride complex (black curve) was recorded in 50 mM potassium phosphate buffer, pH 8.0, containing 2.0 M potassium chloride at 25 °C. Absorption spectra recorded after addition of 1.38, 3.85, 7.41 and 26.47 mM MTA are shown in the red, blue, green, and cyan curves, respectively. The absorption spectrum calculated for 100% complex formation, as described in Experimental Procedures, is shown in the magenta curve. The inset shows a plots of absorbance changes at 528 nm as a function of the concentration of methylthioacetate. The solid red line was obtained by fitting a theoretical binding curve ($\Delta A_{\text{obs}} = \Delta A_{\text{max}}[\text{ligand}]/(K_d + [\text{ligand}])$) to the data (black circles). Panel B: The red curve is the difference spectrum obtained by subtracting the spectrum of the MSOX•chloride complex from the spectrum calculated for 100% formation of the MSOX•chloride•MTA complex. The blue curve is the corresponding spectral perturbation observed upon binding of MTA to free MSOX in 50 mM potassium phosphate, pH 8.0. The same difference spectrum for 100% formation of the MSOX•MTA binary complex was obtained when the titration of free MSOX was conducted at 25 °C in 50 mM potassium phosphate, pH 8.0 containing 0.667 mM sodium sulfate (data not shown).

**Figure 4.**

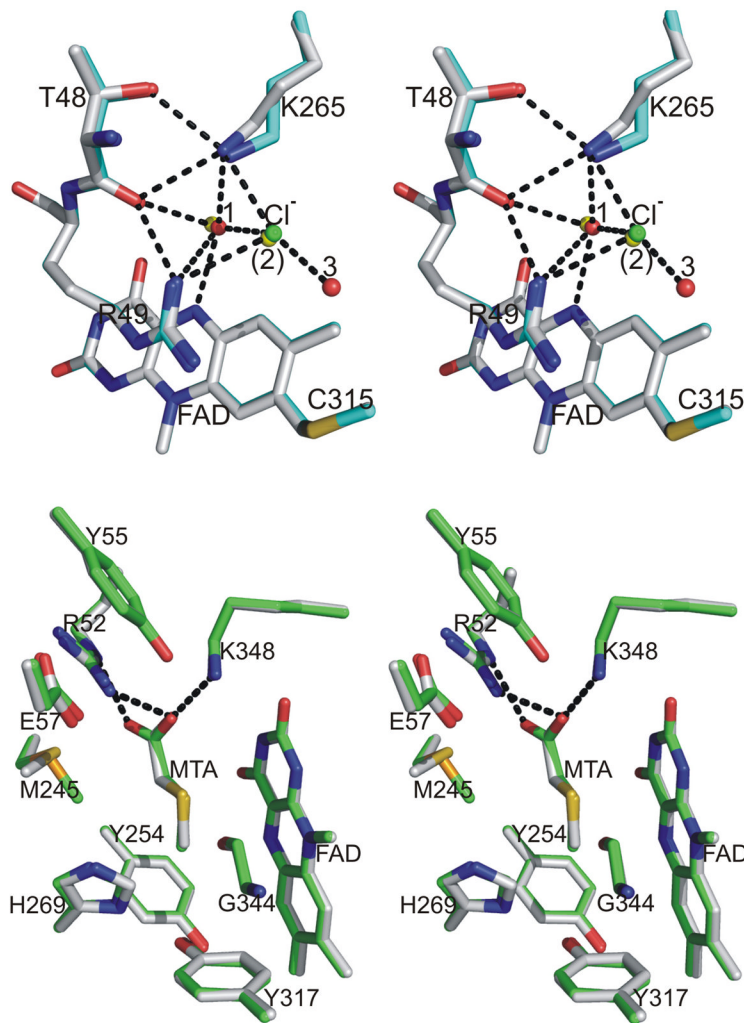
Spectral properties of the binary complex formed with glucose oxidase and chloride. The spectral titration was conducted in 50 mM potassium citrate buffer, pH 3.0, at 25 °C. Panel A: Absorption spectra recorded in the presence of 0, 1.23, 3.62, and 18.37 mM potassium chloride are shown in the black, red, blue, and green curves, respectively. The magenta curve is the spectrum calculated for 100% complex formation, as described in Experimental Procedures. Arrows indicate the direction of the observed spectral change with increasing chloride concentration. The inset shows a plot of absorbance changes at 504 nm as a function of the concentration of chloride. The solid red line was obtained by fitting a theoretical binding curve ($\Delta A_{\text{obs}} = \Delta A_{\text{max}}[\text{ligand}]/(K_d + [\text{ligand}])$) to the data (black circles). Panel B shows the corresponding difference spectra obtained by subtracting the spectrum of free GOX from spectra observed in the presence of chloride.

**Figure 5.**

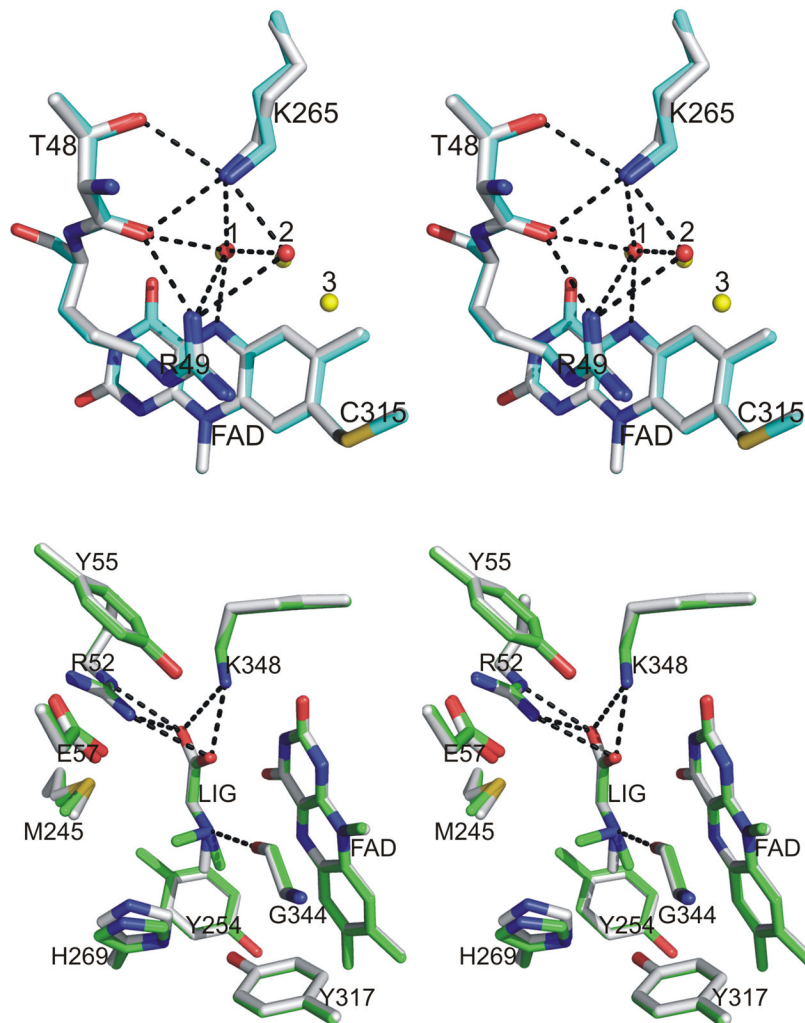
Effect of pH on the stability of the GOX•chloride complex. Dissociation constants of the GOX•chloride complex at different pH values were determined as described in the legend to Figure 4 and Table S2. The solid red line was obtained by fitting a theoretical pH titration curve ($\log Y = \log[(AH^+ + BK_a)/(H^+ + K_a)]$) to the data (black circles).

**Figure 6.**

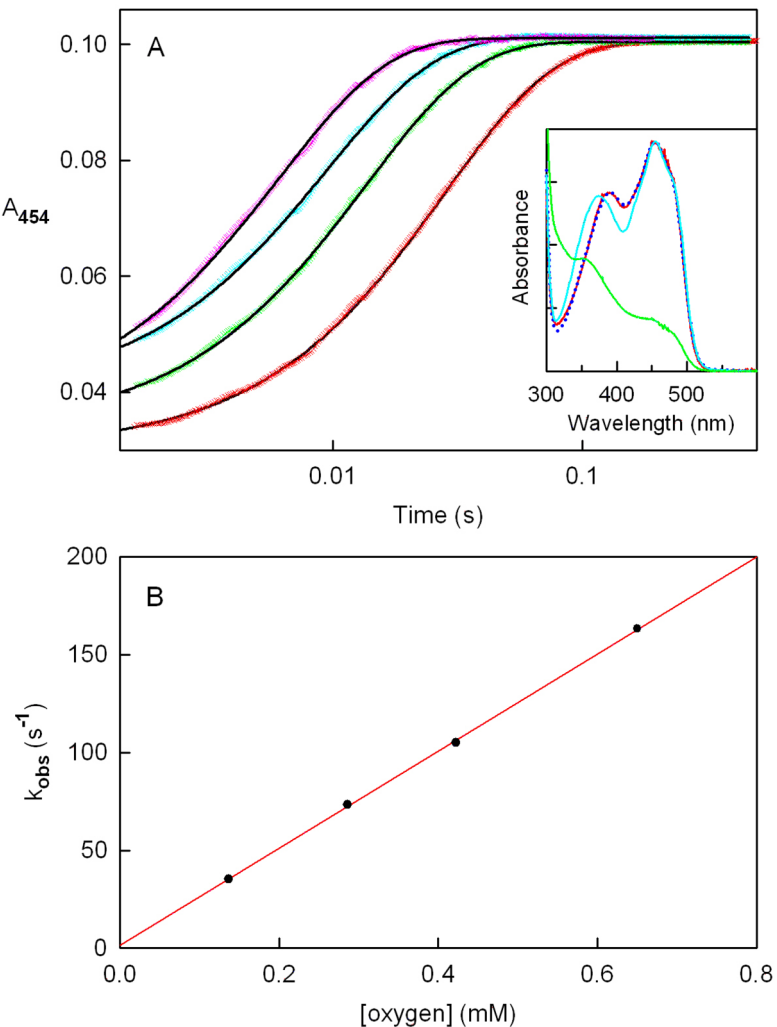
Stereoview comparison of the two active sites in the MSOX•chloride binary complex and ligand-free MSOX (PDB entry code 2GBO, molecule 1). The top panel shows the oxygen activation site above the *si*-face of the flavin ring. Chloride is shown as a green ball. Carbon atoms are white (chloride complex) or cyan (free MSOX), nitrogen atoms are blue, sulfur is gold, and oxygen atoms are red except for waters in free MSOX (yellow balls). Hydrogen bonds in the chloride complex are indicated by dashed lines. The bottom panel shows the sarcosine oxidation site above the *re*-face of the flavin ring. Carbon atoms are white (chloride complex) or green (free MSOX). Waters that occupy the sarcosine binding cavity are shown as red or yellow balls in the chloride complex or ligand-free MSOX, respectively. All other atoms are colored as in the top panel.

**Figure 7.**

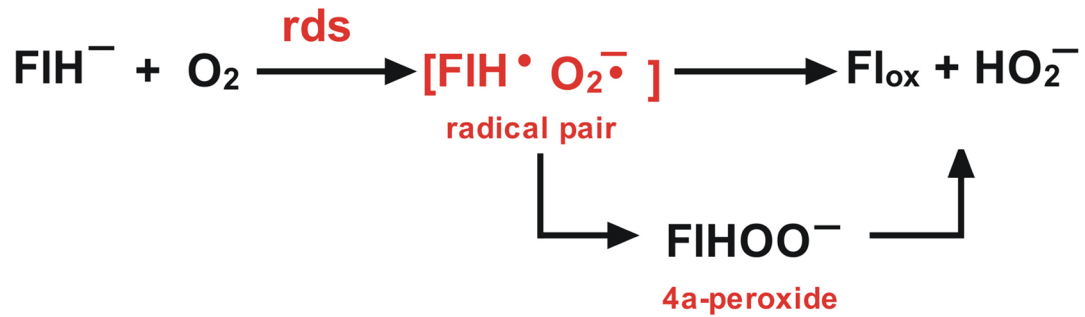
Stereoview comparison of the two active sites in the MSOX•chloride•MTA ternary complex and the MSOX•MTA binary complex (PDB entry code 1EL9). In each panel, hydrogen bonds in the ternary complex are indicated by dashed lines. The top panel shows the region above the *si*-face of the flavin ring with chloride depicted as a green ball. Carbon atoms are white (ternary complex) or cyan (binary complex), nitrogen atoms are blue, sulfur is gold, and oxygen atoms are red except for waters in the binary complex (yellow balls). The bottom panel shows region above the *re*-face of the flavin ring. Carbon atoms are white (ternary complex) or green (binary complex). Nitrogen, oxygen and sulfur atoms are colored blue, red, and gold, respectively.

**Figure 8.**

Stereoview comparison of the two active sites in the reduced MSOX•sarcosine complex and the oxidized MSOX•dimethylglycine complex (PDB entry code 1EL5). In each panel, hydrogen bonds in the reduced enzyme•sarcosine complex are indicated by dashed lines. The top panel shows the region above the *si*-face of the flavin. Carbon atoms are white or cyan in the reduced MSOX•sarcosine complex or the oxidized MSOX•dimethylglycine complex, respectively. Nitrogen atoms are blue, sulfur is gold, and oxygen atoms are red except for waters in the oxidized enzyme•dimethylglycine complex (yellow balls). WAT1 and WAT2 in the MSOX•dimethylglycine complex are largely obscured by the corresponding waters in the reduced MSOX•sarcosine complex. The bottom panel shows the region above the *re*-face of the flavin ring. Carbon atoms are white (reduced MSOX•sarcosine complex) or green (oxidized MSOX•dimethylglycine complex). Nitrogen, oxygen and sulfur atoms are colored blue, red, and gold, respectively. The ligands in the two complexes (LIG) are nearly superimposed.

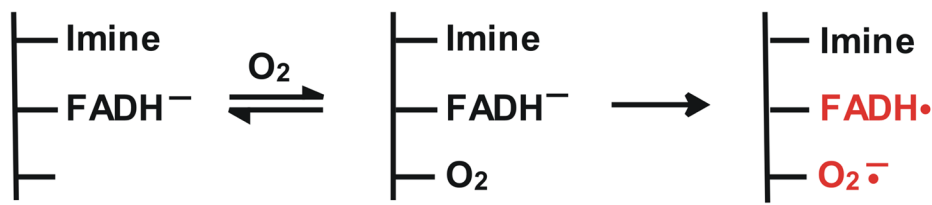
**Figure 9.**

Reaction of reduced MSOX with oxygen in the presence of excess chloride. Reactions were conducted in 50 mM potassium phosphate buffer, pH 8.0, containing 2.0 M potassium chloride at 25 °C and monitored by following the increase in absorption at 454 nm observed upon mixing a reduced anaerobic enzyme solution with buffer containing different concentrations of oxygen in a stopped flow spectrophotometer. Panel A The red, green, cyan and magenta data points (Xs) were obtained for reactions at 0.137, 0.286, 0.423 and 0.650 mM oxygen, respectively (final oxygen concentrations). The solid black lines were obtained by fitting a single-exponential equation ($y = Ae^{-kt} + B$) to the data. The solid green line in the inset shows spectrum of the initial reduced enzyme. The solid red line is spectrum observed after reoxidation with 0.423 mM oxygen. Similar spectra were observed after reaction at each oxygen concentration tested (data not shown). For comparison, control spectra of ligand-free MSOX and the MSOX•chloride complex are shown by the solid cyan and dotted blue lines, respectively. Panel B shows a plot of the observed rate of reoxidation as a function of the oxygen concentration. The red line was generated by linear regression analysis of the data ($r^2 = 0.9997$).



Scheme 1.

Possible paths for hydrogen peroxide formation during oxygen reduction by flavoprotein oxidases.



Scheme 2.

Postulated initial steps in the reaction of the reduced MSOX•imine binary complex with oxygen.

Table 1

Summary of Data Collection and Refinement for MSOX Complexes

	MSOX•Chloride Complex	MSOX•Chloride•MTA Complex	Reduced MSOX•Sarcosine Complex
Data collection			
Wavelength (Å)	1.54	0.9	0.9
Space group	P2 ₁	P2 ₁	P2 ₁
No. molecules per asymmetric unit	2	2	2
Res. Range (last shell) (Å)	40-1.9	40-1.85	40-1.75
No. observations	183643	407063	322755
Unique observations	54598	56973	70527
Completeness (last shell) (%)	97.9 (78.7)	94.7 (92.6)	98.1 (97.4)
R _{merge} ^a (last shell) (%)	6.9 (24.3)	8.1 (54.9)	9.5 (47.2)
I/σ(I) ^b (last shell)	15.8 (2.8)	19.4 (3.7)	14.1 (2.4)
Refinement			
Resolution (Å)	40-1.9	40-1.85	40-1.75
F /σ(F)	>0	>0	>0
R _{crys} ^c	0.184	0.208	0.184
R _{free} ^d	0.212	0.235	0.217
Reflections (working/test)	51025/2724	50679/2713	64556/3208
Protein atoms	6050	5984	5995
Water Molecules	633	528	774
FAD atoms	106	106	106
Ligand atoms	0	12	12
Cl ⁻ ions	4	4	2
Rmsd bond lengths ^e (Å)	0.005	0.007	0.008
Rmsd angles ^e (°)	1.4	1.6	1.6
Rms ΔB (Å ²) (mm/ms/ss) ^f	1.13/1.45/1.94	1.02/1.32/1.74	1.62/2.06/2.81
 protein (Å ²)	24.9	31.2	25.0
 water molecules (Å ²)	32.6	40.1	37.9
 FAD (Å ²)	17.7	24.8	18.0
 Ligand (Å ²)	-	35.5	25.5
 Cl ⁻ ions (Å ²)	21.4	32.0	18.2
Ramachandran plot (%)			
Allowed region	99.5	99.5	99.7
Generously allowed region	0.2	0.2	0.0
Disallowed region	0.3	0.3	0.3

^aR_{merge} = $\sum_h \sum_i |I_i(h) - \bar{I}(h)| / \sum_h \sum_i |I_i(h)|$, where I_i(h) and $\bar{I}(h)$ are the ith and mean measurements of reflection h.

^bI/σ(I) is the average signal to noise ratio for merged reflection intensities.

^cR_{crys} = $\sum_h |F_O(h) - F_C(h)| / \sum_h |F_O(h)|$, where F_O and F_C are the observed and calculated structure factor amplitudes of reflection h.

^dR_{free} is the test reflection data set, about 5 % selected randomly for cross validation during crystallographic refinement.

^eRoot-mean-squared deviation (Rmsd) from ideal bond lengths and angles and Rmsd in B-factors of bonded atoms.

^fmm, main chain to main chain; ms, main chain to side chain, ss, side chain to side chain.

Table 2Properties of binary and ternary complexes formed with MSOX, chloride and MTA^a

Complex	K _d (mM)
MSOX + Cl ⁻ ⇌ MSOX•Cl ⁻	180 ± 10
MSOX•Cl ⁻ + MTA ⇌ MSOX•Cl ⁻ •MTA	4.90 ± 0.07 ^b
MSOX + MTA ⇌ MSOX•MTA	
no additions	2.43 ± 0.02 ^c
plus 667 mM sodium sulfate	1.84 ± 0.01

^aUnless otherwise indicated, titrations were conducted in 50 mM potassium phosphate buffer, pH 8.0, at 25 °C.^bThe titration of MSOX•Cl⁻ complex with MTA was conducted in 50 mM potassium phosphate buffer, pH 8.0, containing 2.0 M potassium chloride, at 25 °C. The observed K_d is attributed to the formation of a MSOX•chloride•MTA ternary complex, as discussed in the text.^cValues of 2.60 mM and 2.88 ± 0.04 mM were obtained in previous studies under the same conditions (13, 45).

Table 3Comparison of MSOX•Chloride or MSOX•Chloride•MTA Crystals with Chloride-free MSOX Crystals^a

enzyme	crystal resolution (Å)	Active Site Loop (Y55–Y61)				External loop (I185-Y192) ^c				WAT2 WAT3				comparison with chloride-free MSOX (RMSD, Å)			
		molecule	Arg52 ^b	Arg52 ^b	Arg52 ^b	molecule 1	molecule 2	molecule 1	molecule 2	ligand-free ^d	MTA complex ^e	ligand-free ^d	MTA complex ^e	ligand-free ^d	MTA complex ^e	ligand-free ^d	MTA complex ^e
Ligand-free MSOX ^d	1.85	1	open	out	A			yes	no								
		2	closed	out and in-like	B			yes	no								
MSOX•MTA ^e	2.00	1	closed	in	A			yes	no ^f								
		2	closed	in	B			no	no ^f								
MSOX•Cl ⁻	1.90	1	closed	in	A			no	yes	0.41	0.21	0.39	0.35				
		2	closed	in	A-like			no	yes	0.51	0.34	0.50	0.47				
MSOX•Cl•MTA	1.85	1	closed	in	A			no	yes	0.51	0.34	0.41	0.38				
		2	closed	in	A-like			no	no ^g	0.50	0.33	0.48	0.47				
reduced MSOX•sarcosine	1.75	1	closed	in	A			yes	no	0.49	0.34	0.51	0.50				
		2	closed	in	A-like			yes	no	0.50	0.33	0.47	0.46				

^aChloride-free refers to the absence of chloride at the oxygen activation site above the si-face of the flavin. As discussed in the text, all crystals contain a chloride ion near the ribityl side chain of FAD.^bThe side chain of Arg52 is found in alternate conformations, one pointing toward the flavin ring ("in") and another pointing away ("out").^cThe external loop is located on the surface of the protein. The configuration of this loop is sensitive to the crystal packing environment (7).^dPDB entry code 2GOO.^ePDB entry code 1EL9^fSimilar to the MSOX•MTA complex, WAT3 is not detected in the MSOX•pyrrole-2-carboxylate complex (PDB entry code 1EL1). WAT3 is, however, found in molecules 1 and 2 in the MSOX•dimethylglycine complex (PDB entry code 1EL5, see Figure 8) and in molecule 1 in the MSOX•2-fluorotyrosine complex (PDB entry code 2GF3).^gThe absence of WAT3 in molecule 2 appears to correlate with the higher B-factor for chloride in molecule 2 (45 Å²) versus molecule 1 (32 Å²) in the ternary complex. The latter is closer to the values observed for chloride in the binary complex (22 and 30 Å² in molecules 1 and 2, respectively).